Electronic Supplementary Material (ESI) for Analyst.

Supplementary Information

A colorimetric chemosensor for sensitive and selective detection of copper (II) ions based on catalytic oxidation of 1-naphthylamine

Rui Cai,[ab] Chaudhary Ammar Shoukat,[ab] Chenqi Zhang,[ab] Xinshuang Gao,[ab] Hanbo Li,[ab] Jiaqi Chen,*[c] Yinglu Ji,*[a] and Xiaochun Wu[ab]

[a]CAS Key Laboratory of Standardization and Measurement for Nanotechnology, National Center for Nanoscience and Technology, Beijing 100190, China.
Email: jiyl@nanoctr.cn
[b]University of the Chinese Academy of Sciences, Beijing 100049, China.
[c]School of Mechanical Engineering, Chengdu University, Chengdu 610000, China.
Email: chenjiaqi@cdu.edu.cn

Supplementary Experiment Information

Chemical reagents. 1-Naphthylamine hydrochloride (α-NA·HCl), nickel chloride hexahydrate ($NiCl_2·6H_2O$), cadmium nitrate tetrahydrate ($Cd(NO_3)_2·4H_2O$), cerium nitrate hexahydrate ($Ce(NO_3)_3·6H_2O$), and hydrogen peroxide (H_2O_2, 30 wt %) were ordered from Aladdin (Shanghai, China). Copper (II) chloride dihydrate ($CuCl_2·2H_2O$) was obtained from Sinopharm Chemical Reagent Co., Ltd (Beijing, China). Manganese (II) chloride tetrahydrate ($MnCl_2·4H_2O$), sodium citrate (Cit), cysteine (Cys), 2-mercaptoethylamine (MEA), 3-mercaptopropionic acid (MPA), and ascorbic acid (AA) was purchased from Sigma-Aldrich (Shanghai, China). Ethylenediaminetetraacetic acid (EDTA) solution (0.5 M, pH 8.0), iron (III) chloride ($FeCl_3$), iron (II) chloride ($FeCl_2$), sodium fluoride (NaF), cobalt nitrate hexahydrate ($Co(NO_3)_2·6H_2O$), chromium(III) nitrate nonahydrate ($Cr(NO_3)_3·9H_2O$), lead chloride ($PbCl_2$), mercury nitrate monohydrate ($Hg(NO_3)_2·H_2O$), and zinc chloride ($ZnCl_2$) were purchased from Macklin (Shanghai, China). Acetate buffers (HAc/NaAc buffer, 0.2 M) with pH values of 2.7, 3.4, 4.5, 5.6, and 6.5 were from Leagene (Beijing, China). Milli-Q water (18 $M\Omega·cm^{-1}$) was used for the preparation of all solutions.

Characterization. The catalytic reactions were carried out in cuvette and monitored using Varian Cary 60 ultraviolet-visible-near infrared (UV-Vis-NIR) spectrophotometer (Agilent Technologies, USA). Raman spectra were recorded from a Renishaw InVia Raman microscope.

Supplementary Figure Information

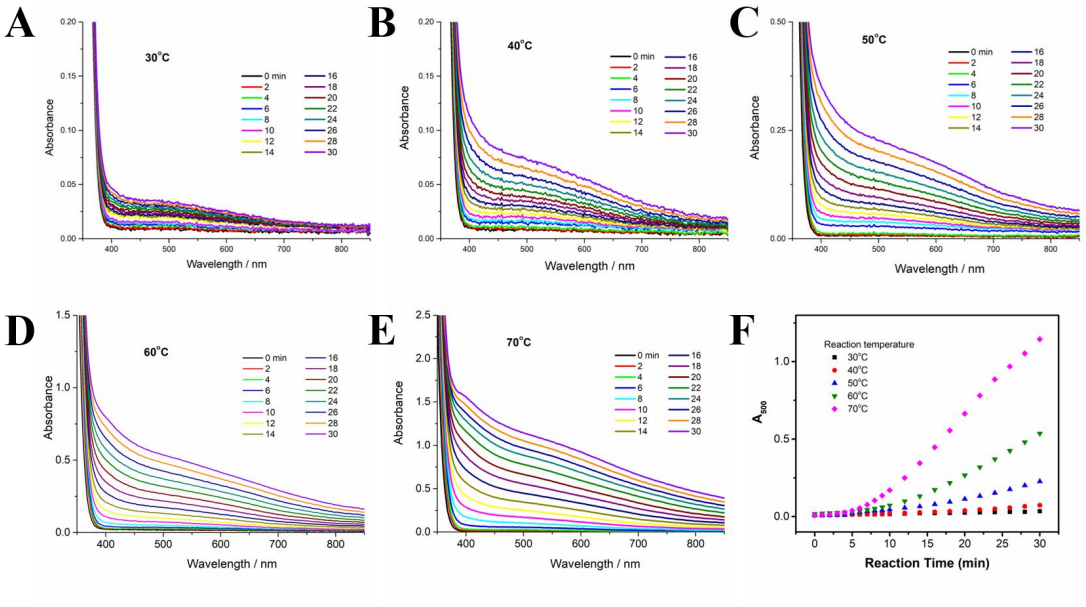

Figure S1. Effect of reaction temperature on the formation of the PNA. Evolutions of UV-vis absorption spectra during α-NA oxidation by H_2O_2 in the presence of 5 μM Cu^{2+} at reaction temperature of (A) 30 °C, (B) 40 °C, (C) 50 °C, (D) 60 °C, and (E) 70 °C, respectively. (F) Initial reaction rates at different temperatures. [α-NA] = 10 mM, [H_2O_2] = 10 mM, and [Cu^{2+}] = 5 μM.

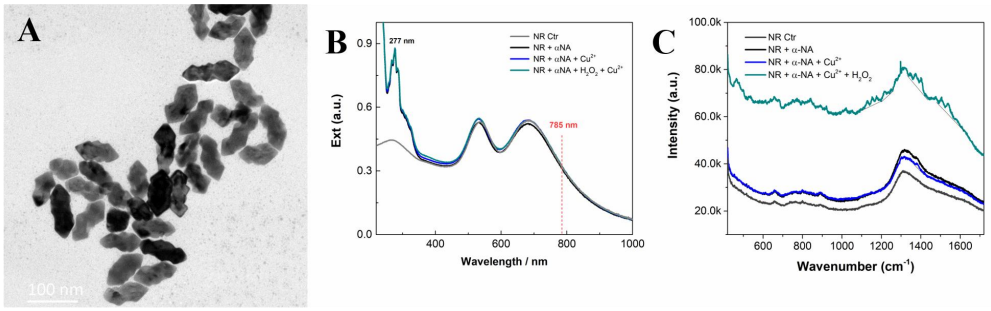

Figure S2. SERS characterization of PNA formation. (A) TEM image of nanorods. Extinction spectra of (B) NR suspensions before and after incubation with three solutions and corresponding SERS spectra (C) excited using a 785 nm laser.

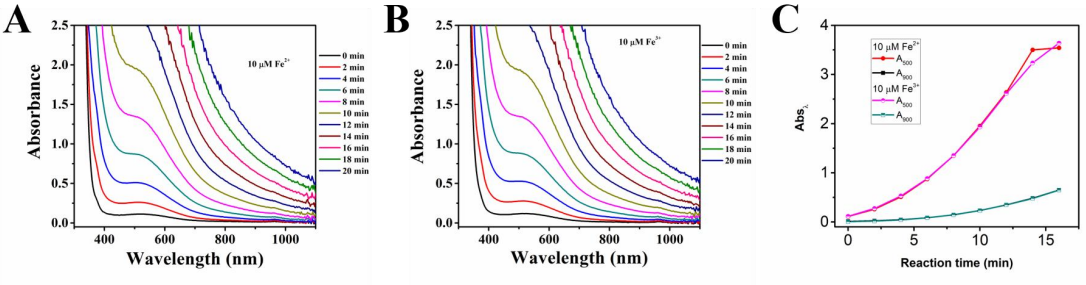

Figure S3. Fe^{2+}- or Fe^{3+} -catalyzed formation of PNA. A, B) Evolution of UV-vis absorption spectra during α-NA oxidation by H_2O_2 in the presence of 10 μM Fe^{2+} or 10 μM Fe^{3+} in 0.1 M

HAc/NaAc (pH4.5) buffer at the reaction temperature of 50 °C. [α-NA] =10 mM, [H_2O_2] = 10 mM. C) A_{500} and A_{900} vs reaction time.

Fe-Fenton reactions

$Fe^{2+} + H_2O_2 \rightarrow Fe^{3+} + OH^- + \cdot OH$ (eq.1)

$Fe^{3+} + H_2O_2 \rightarrow Fe^{2+} + \cdot OOH + H^+$ (eq.2)

In our case, owing to the high concentration of H_2O_2, the conversion of Fe^{3+} to Fe^{2+} is not rate-limiting step (eq.2). Therefore, there is no obvious difference between the formation rate of the PNA catalyzed by Fe^{2+} and Fe^{3+}.

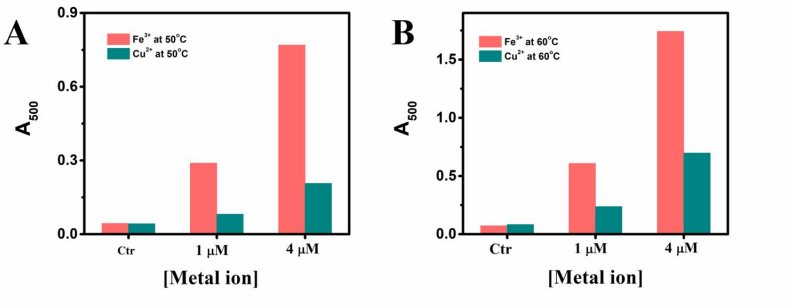

Figure S4. Comparison of Fe^{3+} and Cu^{2+} in catalyzing the oxidative polymerization of α-NA. (A) 50 °C 20 min. (B) 60 °C 20 min. [α-NA] =10 mM, [H_2O_2] = 10 mM.

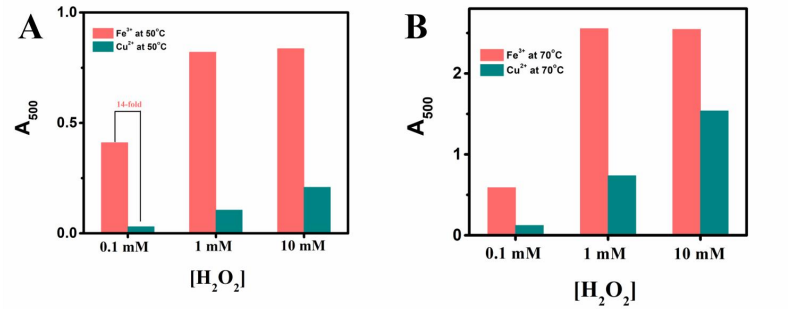

Figure S5. Different H_2O_2 concentration dependence of Fe^{3+} and Cu^{2+} in catalyzing the oxidative polymerization of α-NA. A) Reaction temperature of 60 °C for 20 min. B) Reaction temperature of 70 °C for 20 min. Reaction conditions: [α-NA] =10 mM, [Fe^{3+}] = 4 μM. [Cu^{2+}] = 4 μM.

At 0.1 mM H_2O_2, $Abs_{500\ nm}$ from Fe^{3+}-catalyzed system is ca 15-fold of that from Cu^{2+}-catalyzed system. Therefore, 0.1 mM H_2O_2 can be used to detect Fe^{3+}. At 1 mM H_2O_2, Fe^{3+}-catalyzed system reached saturation with H_2O_2 concentration, corresponding to a molar ratio of [H_2O_2]/[Fe^{3+}] of 250. In contrast, a linear concentration dependence between 0.1 mM to 10 mM was observed for Cu^{2+}-catalyzed system, which may be used for H_2O_2 detection.

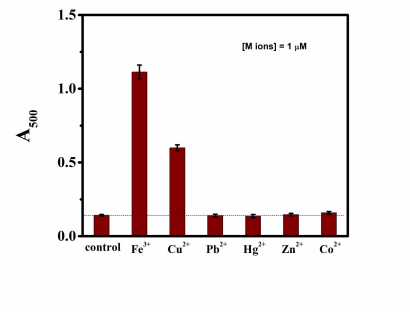

Figure S6. A_{500} of reaction solutions obtained at the default reaction condition in the presence of different metallic ions at 1 μM.

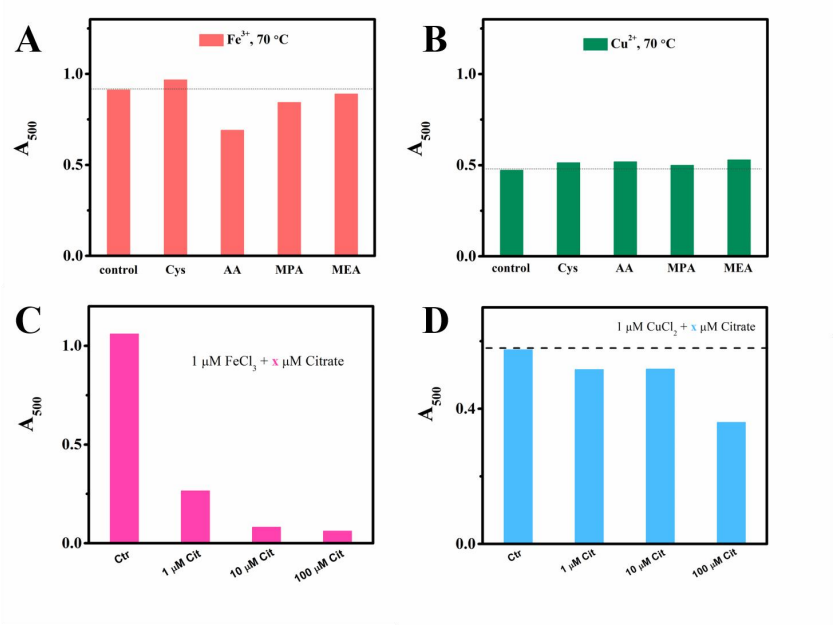

Figure S7. Effect of commonly employed masking agents of Fe^{3+} (1 μM) and Cu^{2+} (1 μM) on inhibiting their catalytic activities for the oxidative polymerization of α-NA at default reaction conditions. (A, B) In the absence or presence of 10 μM blocking agent. (C, D) Effects of citrate concentration.

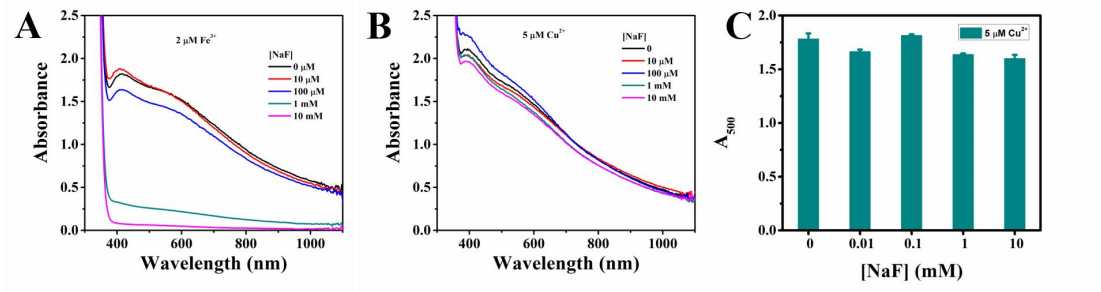

Figure S8. Effect of NaF concentration on catalytic activity. Absorbance spectra for 2 μM Fe^{3+} (A) or 5 μM Cu^{2+} (B) obtained at the default reaction conditions. (C) A_{500} vs NaF concentration in Cu^{2+}-catalyzed reaction.

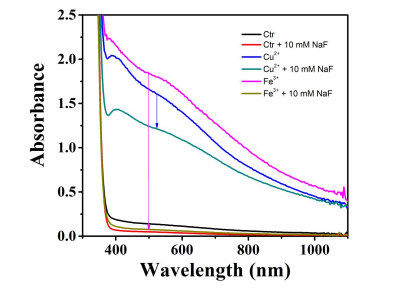

Figure S9. UV-vis absorption spectra of α-NA oxidation at the default reaction condition catalyzed by Cu^{2+} or Fe^{3+} in the absence or presence of 10 mM NaF, respectively. Control groups were reaction solutions without adding Cu^{2+} or Fe^{3+}.

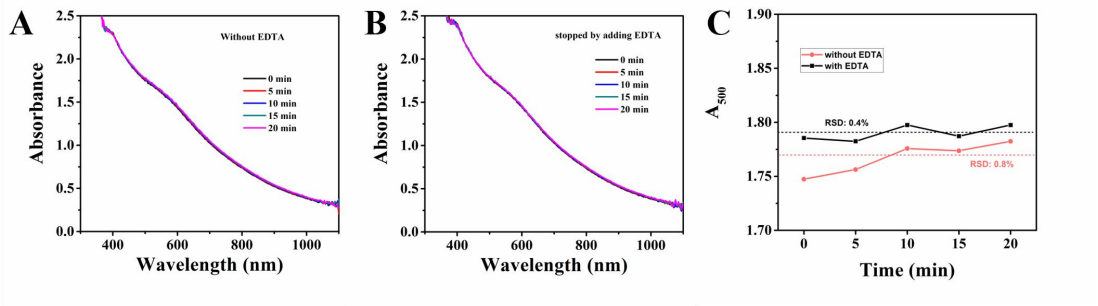

Figure S10. Signal stability at room temperature after cooling (A) and after cooling and chelating with EDTA (B), respectively. A_{500} vs time (C). Default detection conditions in the presence of 5 μM Cu^{2+}.

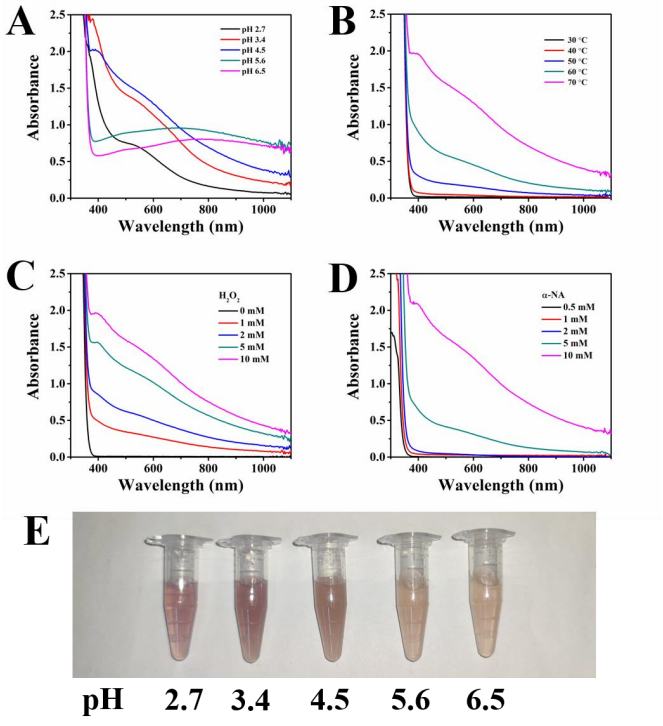

Figure S11. Effect of (A) pH, (B) reaction temperature, (C) H_2O_2 concentration, and (D) α-NA

concentration on the UV-vis absorption spectra of α-NA oxidation by H_2O_2 in the presence of Cu^{2+}. (E) Corresponding photographs of reaction solutions after the reaction at pH 2.7, pH 3.4, pH 4.5, pH 5.6, and pH 6.5, respectively. Unless specified, the default reaction condition was used.

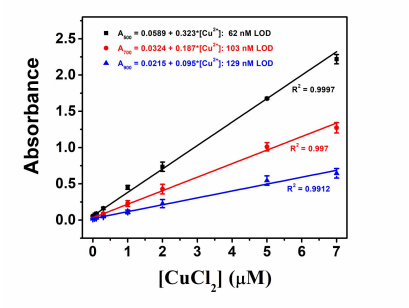

Figure S12. Comparison of calibration plots of A_{500}, A_{700}, and A_{900} vs Cu^{2+} concentration.

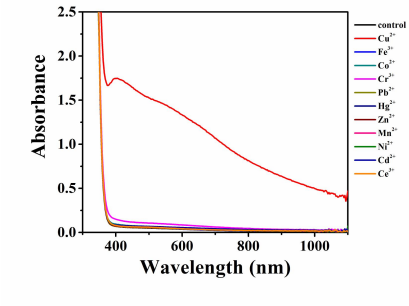

Figure S13. Absorption spectra of α-NA after reaction at the default detection condition in the presence of different metallic cations. $[Cu^{2+}]$ = 5 μM, $[M^{2+}$or $M^{3+}]$ = 50 μM. Control group was reaction solutions without adding metallic cations.

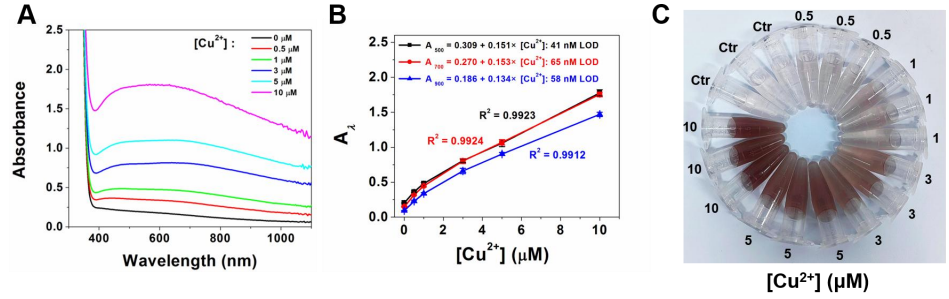

Figure S14 Detection of copper (II) ions in the presence of tap water. (A) Absorbance spectra of reaction solutions at different concentrations of copper (II) ions after reacting at 70°C 20 min and then stopped by ice cold water. (B) A_{500}, A_{700}, and A_{900} vs concentration of added copper (II) ions. (C) Photographs of three parallel experiment samples containing 100 μl tap water after reaction at the default reaction condition.

Supplementary Table Information

Table S1 Comparison of colorimetric assays and non-colorimetric methods for Cu^{2+} detection

Sensing mechanism	Linear range	LOD	Reference
Cation exchange of copper ion with zinc ion in ZnS shell of the ZnO@ZnS NP to form a colored CuS shell	15–1500 μM	15 μM	1
Formation of a colorless complex between yellow naphthalenediimideamphiphile and Cu^{2+}	——	260 nM	2
Cu^{2+}-induced aggregation of AgNP modified by 1,3-alternate calix[4]arene	——	2.5 μM	3
Cu^{2+}-catalysed TMB oxidation by H_2O_2 (signal amplification via forming Cu^{2+}-G-quadruplex DNA complex)	5–60 μM (0.1–5 μM)	2.6 μM (76 nM)	4
Cu^{2+}-assisted TMB oxidation in AgNP suspension containing $Na_2S_2O_3$	1–100 μM	100 nM	5
Cu^{2+}-triethylamine complex –catalyzed TMB and dopamine oxidation by H_2O_2	0.0625–8.0 μM	62.5 nM	6
Cu^{2+}-catalyzed oxidation coupling of α -naphthylamine via Cu-Fenton mechanism	0.05–7 μM	62 nM	This work
Electrochemical sensor based on current change of Pi-A/RGO modified electrode upon selective binding of Cu^{2+} to Pi-A	0.08–4.7 μM	10.5 nM	7
Fluorescence probe based on Cu^{2+}-catalyzed hydrolysis reaction	0-10 μM	36 nM	8
Turn-on red-emitting fluorescence probe based on selective cleaving of picolinoyl ester by Cu^{2+}	0.02-8 μM	4 nM	9

References

1 A. Sadollahkhani, A. Hatamie, O. Nur, M. Willander, B. Zargar and I. Kazeminezhad, *ACS Appl. Mater. Interfaces*, 2014, **6**, 17694-17701.

2 N. V. Ghule, R. S. Bhosale, A. L. Puyad, S. V. Bhosale and S. V. Bhosale, *Sens. Actuators, B*, 2016, **227**, 17-23.

3 G. Nsengiyuma, R. Hu, J. Li, H. Li and D. Tian, *Sens. Actuators, B*, 2016, **236**, 675-681.

4 X. Wei, H. Xu, W. Li and Z. Chen, *Sens. Actuators, B*, 2017, **241**, 498-503.

5 Z. Zhang, W. Zhao, C. Hu, D. Guo and Y. Liu, *J. Sci.: Adv. Mater. Devices*, 2022, **7**, 100420.

6 H. Zhou, T. Chai, L. Peng, W. Zhang, T. Tian, H. Zhang and F. Yang, *Dyes Pigm.*, 2023, **210**, 111028.

7 L. Yang, N. Huang, L. Huang, M. Liu, H. Li, Y. Zhang, S. Yao, *Anal. Methods*, 2017, **9**, 618-624.

8 Z. Zhou, S. Chen, Y. Huang, B. Gu, J. Li, C. Wu, P. Yin, Y. Zhang, H. Li, *Biosensors and Bioelectronics*, 2022, 198, 113858

9 Z. Zhou, H. Tang, S. Chen, Y. Huang, X. Zhu, H. Li, Y. Zhang, S. Yao, *Food Chemistry*, 2021, **343**, 128513.